Hindawi
Advances in Civil Engineering
Volume 2023, Article ID 5510612, 14 pages
https://doi.org/10.1155/2023/5510612

Research Article

The Deformation, Failure Mechanisms, and Stability Control of the Surrounding Rock of Deep Cross-Measure Roadway: A Case Study

Wenzheng Du, Rui Pan, and Hongjin Sun

Anhui Province Key Laboratory of Building Structure and Underground Engineering, Anhui Jianzhu University, Hefei 230601, China

Correspondence should be addressed to Rui Pan; pr5813050@126.com

Received 19 April 2023; Revised 12 June 2023; Accepted 29 July 2023; Published 11 August 2023

Academic Editor: Chu Zhaofei

In view of the difficulty in controlling the surrounding rock stability of deep cross-measure roadways, a deep cross-measure roadway of the Wanfu coal mine, a typical high-stress mine, was monitored on site and analyzed under the original support scheme. The findings show that the degrees of deformation and failure of the cross-measure roadway varied under different working conditions and that the roadway deformation and failure were mainly characterized by a high fragmentation degree and a large failure range of the surrounding rock and the frequent failure of support components. Considering that the different parts of the cross-measure roadway are located in different lithostratigraphic units, establishing a numerical model of the cross-measure roadway under different working conditions; analyzing the deformation pattern of the surrounding rock of the roadway, the plastic range, and the morphological change pattern; and clarifying the deformation and failure mechanisms of the cross-measure roadway based on field monitoring results. On this basis, two types of evaluation indicators, that is, the deformations of the surrounding rock and the plastic ranges in the four typical parts (roof, shoulder, floor, and sidewalls) of the roadway, were selected to rate the stability of the roadway under different working conditions. Grouting reinforcement-based targeted control countermeasures are proposed to improve the surrounding rock stability. Subsequently, numerical analysis and field application of these control countermeasures were carried out to solve the problem of controlling the surrounding rock stability of deep cross-measure roadways.

1. Introduction

With the continuous increase in mining depth and intensity, many roadways are difficult to support, including high-stress roadways, roadways with soft and broken or extremely broken surrounding rock, roadways with extremely large cross-sections, gob-side roadways, and cross-measure roadways [1–3]. Cross-measure roadways are the development roadways of coal mines. During excavation, a cross-measure roadway passes through two or more different lithostratigraphic units; as a result, the degree of deformation and failure of the roadway varies in different intervals due to the differences in ground stress, support method, and lithology. Therefore, it is necessary to study the deformation and failure patterns of cross-measure roadways and to carry out targeted evaluation and control of the surrounding rock stability under different working conditions to ensure safe mine production and construction.

In terms of the deformation and failure of the soft and hard interbedded rock masses of cross-measure roadways, Huang et al. [4] used interbedded sandstone–mudstone rock masses as the study object. They built similar soft and hard interbedded rock masses with different bed thickness ratios and inclination angles to analyze the effect of confining pressure, bed thickness ratio, and rock bed inclination angle on the mechanical properties and failure mechanisms of soft and hard interbedded rock mass. Liu et al. [5] conducted laboratory direct shear tests under constant normal pressure for two types of typical structural planes of soft and hard interbedded rock mass ("soft + hard" and "hard + soft + hard"),

proposed the corresponding shear strength estimation formula, and verified the formula through examples. Li et al. [6] used the soft and hard interbedded composite rock mass in the underground powerhouse area of the Jinping I hydropower station as the research object to simulate the mesoscopic fracture processes of rock samples under uniaxial compression. Their results provide a theoretical basis for the study of mechanical properties of interbedded composite rock mass in underground projects. Using an improved rigid spring method, Yao et al. [7] proposed a stepwise interpolation algorithm for the automatic generation of computational grids and used it to simulate the initiation and propagation of mesofractures in soft and hard interbedded rock materials under different confining pressures. Huang and Cheng [8] established a soft and hard interbedded roadway floor model and analyzed the influence of the soft and hard properties of the rock mass on the stress distribution and failure characteristics of the roadway floor. In terms of the stability evaluation of the surrounding rock of the cross-measure roadway, Barton and Grimstad [9], a Norwegian scholar, proposed the Q-system for rock mass classification based on the field measurement data and the influences of ground stress. Bieniawski [10] established a rock mass rating (RMR) system considering several factors that have the most significant impact on surrounding rock stability. Wang et al. [11] used the fuzzy clustering method to classify the coal roadway based on field survey data for the stability control of the surrounding rock of the large cross-section coal roadway in the Zhaozhuang Mine, which effectively guided the design of the support parameters for the surrounding rock of the coal roadway. Zhu and Ma [12] selected six main indicators that affect the classification of the surrounding rocks of mining roadways and used support vector machine classification to perform classified prediction and verification on the surrounding rock of four mining roadways in the Pingdingshan mining area. Jiao et al. [13] quantitatively evaluated the stability of roadway surrounding rock in small- and medium-sized coal mines and proposed a grading support method and the support parameters for roadway surrounding rock based on prestressed bolt support, which ensured the roadway stability during excavation and mining. Liu et al. [14] established an unascertained measurement function based on the measured data, analyzed the uncertain influencing factors in the roadway stability evaluation, and obtained the roadway stability evaluation results according to the credible degree recognition criteria. Yu and Peng [15] screened four quantitative indicators that affect the roadway surrounding rock stability, categorized five types of stable and rational support methods, and solved the difficulty in evaluating the surrounding rock stability in coal mine design. To control the surrounding rock stability of cross-measure roadways, Sun et al. [16] proposed the "bolt + cable + reinforced beam + metal mesh + grouting" repair plan based on the +980 m track roadway of the Faer coal mine, which effectively controlled the serious deformation and fragmentation of the surrounding rock of the cross-measure roadway after repeated mining of multiple coal seams. Yang et al. [17] analyzed the deformation and failure characteristics of the surrounding rock of a steeply inclined soft and hard interbedded roadway and proposed a method to strengthen the support at key locations using cables and base angle bolts based on bolt–mesh–cable coupling support, which successfully controlled the large deformation of the surrounding rock. Wang et al. [18] studied the asymmetric deformation and failure characteristics of the surrounding rock of a deep inclined cross-measure roadway and proposed an asymmetrically coupled support strategy consisting of bolts, meshes, cables, and base angle bolts for reinforced support of key locations, which effectively inhibited the asymmetric deformation of the surrounding rock. Jia et al. [19] revealed the distribution pattern and roof caving mechanism of the butterfly-shaped plastic zone in a layered roof roadway with high deviatoric stress and proposed that the key to preventing roof caving in this type of roadway is that the bolt (cable) is longer than the boundary of the plastic zone and can withstand large deformation without breaking.

Previous studies have made certain achievements in the control of the surrounding rock stability of the cross-measure roadway. However, due to the complex and changeable engineering and geological conditions at the site, more studies must be conducted on the deformation and failure characteristics of the surrounding rock of the cross-measure roadway under different working conditions, including stability evaluation and targeted control countermeasures. Based on the previous research, this study analyzed the deformation and failure mechanisms of a deep cross-measure roadway of the Wanfu coal mine, a typical high-stress mine in China, evaluated the stability of the cross-measure roadway under different working conditions, and proposed the targeted control countermeasures to ensure the cross-measure roadway stability to provide a reference for solving this type of problem related to controlling the stability of roadway surrounding rock.

2. Project Background

2.1. Project Overview. The Wanfu coal mine is located in Heze City, Shandong Province, China. It belongs to the Juye Coalfield. The Wanfu coal mine is the largest mine in China, with an alluvium of ~750 m thick. It is also a typical deep mine with high stress. Its maximum principal stress is as high as 58 MPa. The designed production capacity of this mine is 1.8 million t/a. Two levels of development are used: the level of the shaft inset is −820 m, and the development level is −950 m.

South of the shaft inset (−820 m), a group of main lanes are arranged on the −820 m level, namely, the number 1 track main roadway, the number 2 track main roadway, the southern belt conveyer main roadway, and the southern ventilation main roadway, which are used for auxiliary transportation, coal transportation, and ventilation. The number 1 track main roadway is the object of the present study. The maximum horizontal stress in the area where the number 1 track main roadway is located is 37.1 MPa, forming a 60° angle with the roadway; the minimum horizontal stress is 24.5 MPa, the vertical stress is 23.34 MPa, and the lateral

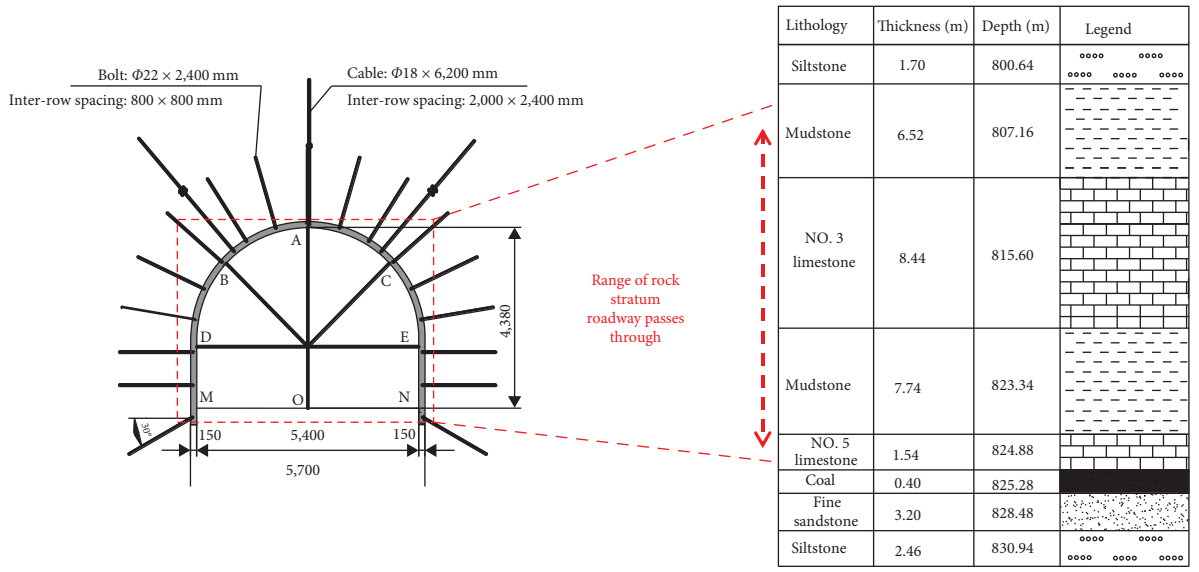

Figure 1: Location and original supporting scheme of research roadway.

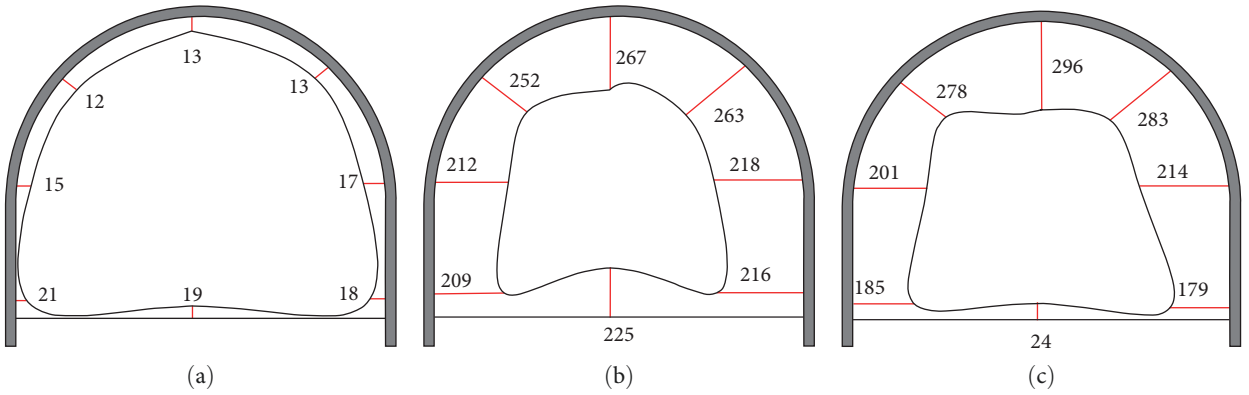

Figure 2: Roadway final shape of typical working conditions. (a) Limestone interval, (b) mudstone interval, and (c) mudstone and limestone interval.

pressure coefficient is 1.58. Therefore, the number 1 track main roadway is a high-stress roadway dominated by tectonic stress. Figure 1 shows the design of the cross section support of the number 1 track main roadway and the conditions of the strata that it passes through.

As shown in Figure 1, the number 1 track main roadway passes through soft and hard rock strata (including number 5 limestone, mudstone, number 3 limestone, and mudstone strata) at the −820 m level during excavation. It is a typical cross-measure roadway. The cross section of the roadway is in a shape of straight wall and semicircular arch with a net width of 5,400 mm and net height of 4,380 mm. The bolt model is $\Phi 22 \times 2{,}400$ mm with interrow spacing of 800×800 mm; the cable model is $\Phi 18 \times 6{,}200$ mm with interrow spacing of $2{,}000 \times 2{,}400$ mm; and the C20 concrete is sprayed on the roadway surface with thickness of 150 mm.

2.2. Analysis on Deformation and Failure of Surrounding Rock under Original Support Scheme. To clarify the deformation and failure characteristics of the surrounding rock of the roadway under the original support scheme, the deformation of the surrounding rock of the roadway and the stress on the support components were monitored and analyzed on site. As shown by the 90-day field monitoring results, the original support scheme cannot meet the needs of surrounding rock stability control unless the entire roadway is located in the limestone strata, and the roadway has the following main forms of on-site deformation and failure:

(1) There are different lithostratigraphic units along the strike of the roadway, and the degree of deformation and failure of the surrounding rock varies under different working conditions. During roadway excavation, the roadway in the limestone interval had an average surrounding rock deformation of 16 mm and high stability, as shown in Figure 2(a); the surrounding rock of the roadway in the mudstone interval showed a large overall deformation, with an average deformation of 232.8 mm, as shown in Figure 2(b); when the roof and sidewalls of the roadway were in the mudstone interval and the floor of the roadway was in the limestone interval, the roof and sidewalls

(a) (b)

Figure 3: Deformation and failure of roadway under original support scheme. (a) Deformation and failure of surrounding rock and (b) Failure of support component.

showed large deformations, and the floor had high stability, as shown in Figure 2(c).

(2) The surrounding rock was highly fragmented and damaged extensively. The damage range of the roadway in the mudstone interval exceeded the length of the bolt, and the damage range in some locations even exceeded the length of the cable. In particular, the mudstone was easily broken after excavation disturbance due to its low strength, resulting in cracking of the spray layer and tearing of the metal mesh. In some locations, the spray layer fell off in chunks, and small-scale roof caving and leakage occurred, as shown in Figure 3(a).

(3) Failures of support components, such as bolt (cable) breakage and bolt plate detachment from the rock surface, occurred frequently, as shown in Figure 3(b). The overall stress on the bolts was relatively low, and during the on-site construction of the anchoring support system, the surrounding rock in the borehole was prone to collapse, and the surrounding rock on the borehole wall tended to fall off, resulting in a noncompact filling between the bolt, the anchoring agent, and the surrounding rock. Therefore, the supporting system could not function effectively.

Based on the above analysis, this study carried out two main lines of research: (1) establishing a numerical model of the cross-measure roadway under different working conditions; analyzing the deformation pattern of the surrounding rock of the roadway, the plastic range, and the morphological change pattern; and clarifying the deformation and failure mechanisms of the cross-measure roadway based on field monitoring results; (2) analyzing the stability of the cross-measure roadway and designing the targeted support schemes to solve the problem of surrounding rock stability control of the cross-measure roadway, thus providing a reference for roadway stability control under similar conditions.

3. The Deformation and Failure Mechanisms of the Surrounding Rock of Deep Cross-Measure Roadway

3.1. Numerical Test Scheme Design and Model Establishment. According to the on-site control effect of the stability of the rock surrounding the roadway under the original support scheme and the histogram of the rock strata shown in Figure 1, this section classifies the siltstone, limestone, and fine sandstone as hard rocks and classifies the mudstone and coal as soft rocks. As shown in Figure 4, the numerical models of six working conditions numbered C1–C6 were designed using the cross-section size of the roadway and the bolting and shotcrete support parameters as invariants and the combinations of different soft- and hard-rock strata as the variables to study the deformation and failure patterns of the surrounding rock under different working conditions of the cross-measure roadway.

The model dimension is 40 m × 50 m × 1.6 m (width × height × thickness), and is disassembled by hexahedron elements with a total of 1,16,800 units and 1,33,164 nodes, as shown in Figure 5. The maximum horizontal stress is decomposed into the direction of vertical roadway and parallel roadway, and the stress size is 32.13 MPa and 18.55 MPa, respectively. The constraint is carried out from x, y, and z three directions at the bottom, and from x and y directions at the two sides, in front and rear, 23.8 MPa compensation load is applied on the upper part of the model.

Mohr–Coulomb criterion is used on the surrounding rock and spray layer, and the mechanical parameters are shown in Table 1. After the completion of the excavation, concrete spray layer, anchor bolts, and cables are installed. The concrete spray layer is close to the surface of the surrounding rock with a thickness of 150 mm. The model is arranged with two rows of bolts and one row of cable; and the mechanical parameters are shown in Table 2.

3.2. Result Analysis. In this section, the surface displacements of the roof, floor, shoulder, and sidewalls of the roadway and the range and morphology of the plastic zone were comparatively analyzed. The deformation of the surrounding rock refers to the maximum displacement of the surrounding rock. The range of the plastic zone refers to the maximum depth of the plastic zone, and the morphology of the plastic zone refers to the distribution characteristics of the plastic zone under different working conditions.

3.2.1. Comparative of Surrounding Rock Deformation under Different Working Conditions. Figure 6 shows the calculation results of the surrounding rock deformation under different working conditions.

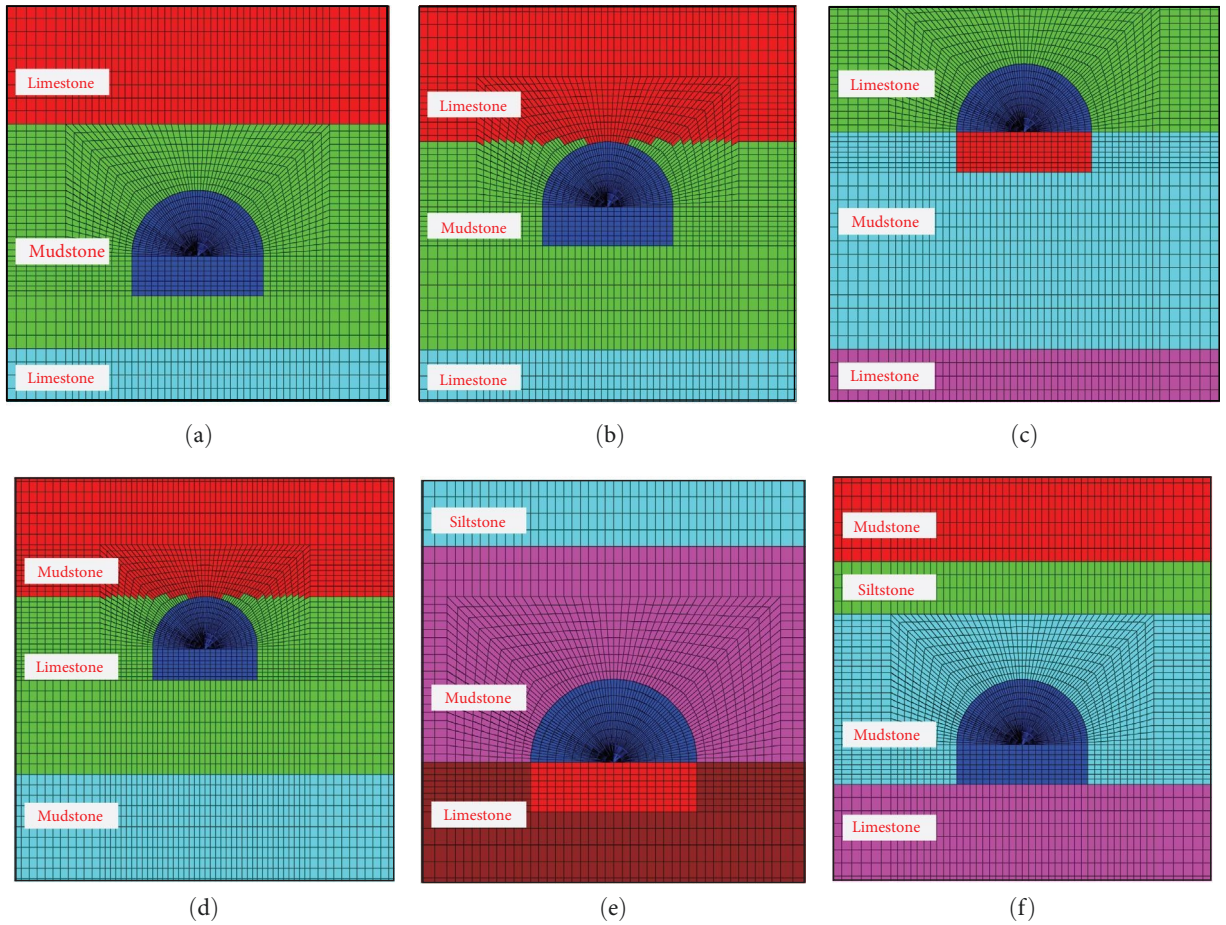

Figure 4: Numerical model of different working conditions. (a) C1, (b) C2, (c) C3, (d) C4, (e) C5, and (f) C6.

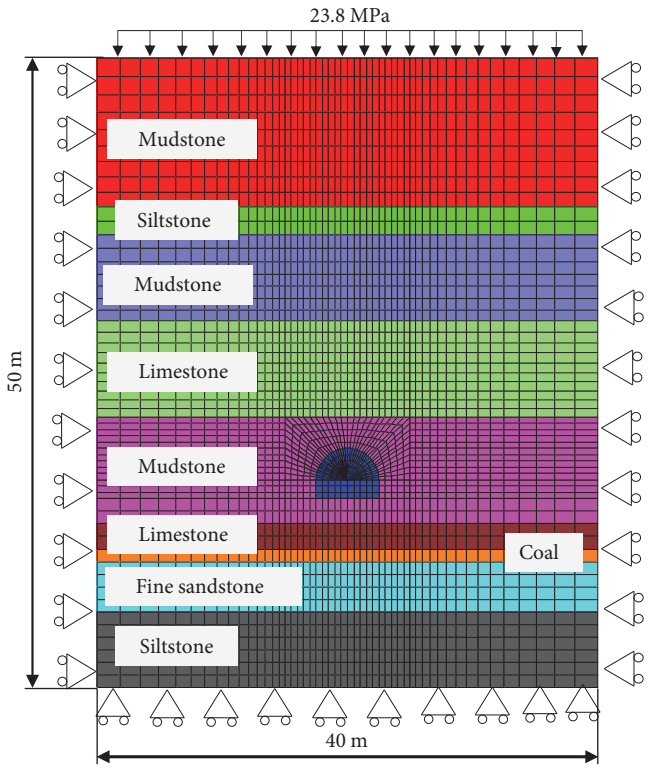

Figure 5: Numerical calculation model.

Table 1: Mechanical parameters of surrounding rock and spray layer.

Lithology	E (MPa)	μ	c (MPa)	φ (°)	σ_t (MPa)
Siltstone	8,950	0.26	3.8	31	0.34
Limestone	27,800	0.25	5.3	30	0.58
Fine sandstone	10,170	0.25	3.5	32	0.43
Mudstone	1,700	0.32	1.2	33	0.35
Coal	1,500	0.30	1.0	34	0.25
Spray layer	23,000	0.20	1.5	35	1.00

The comparative analysis shows that:

(1) The roof, floor, shoulder, and sidewalls of the roadway are located in different rock strata under different working conditions, which results in inconsistent surrounding rock deformation patterns at different parts of the roadway. The roof displacements in working conditions C1–C6 are 240.9, 47.2, 33.8, 198.8, 250.7, and 270.5 mm, respectively, following the order C6 > C5 > C1 > C4 > C2 > C3. The floor displacements in working conditions C1–C6 are 201.7, 278.5, 295.2, 9.0, 9.4, and 10.9 mm, respectively, following the order C3 > C2 > C1 > C6 > C5 > C4. The shoulder displacements in working conditions

Table 2: Parameters of support components.

Support component	Size (mm)	Poisson's ratio μ	Yielding strength σ_s (MPa)	Ultimate strength σ_b (MPa)	Elasticity modulus E (GPa)	Pretension F (kN)
Bolt	$\Phi 22 \times 2{,}400$	0.3	500	700	200	30
Cable	$\Phi 18 \times 6{,}200$	0.3	1,500	1,860	195	120
Grouting bolt	$\Phi 32 \times 2{,}500$	0.31	400	600	180	35
Grouting bolt	$\Phi 32 \times 2{,}000$	0.31	400	600	180	35

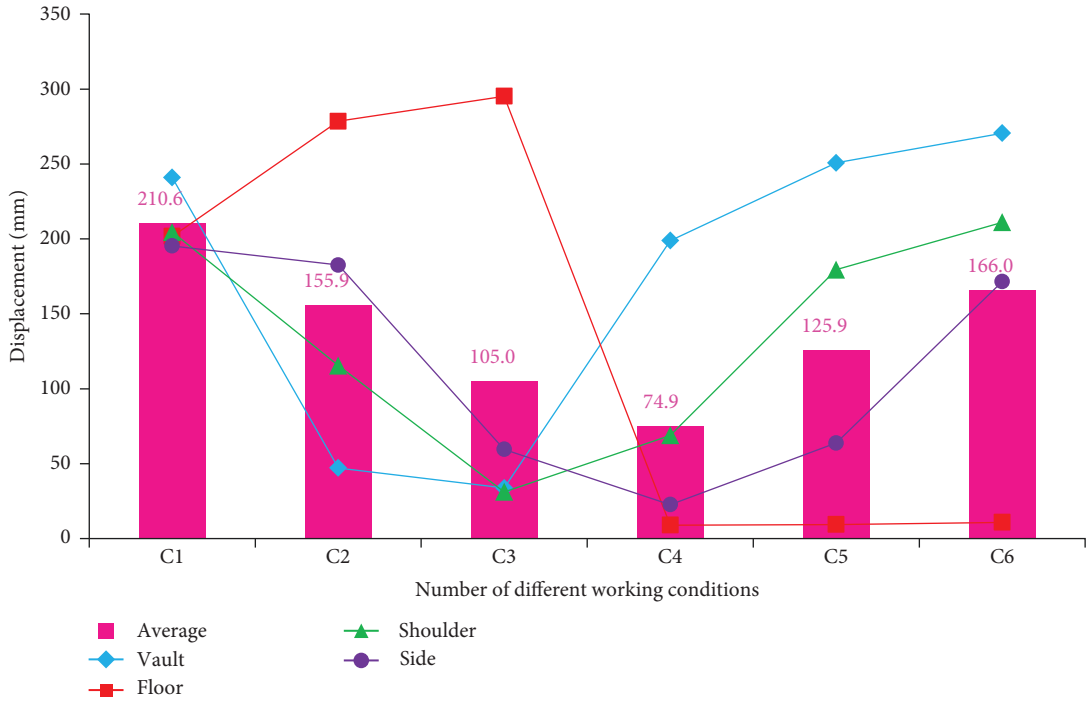

Figure 6: Maximum displacement of different working conditions.

C1–C6 are 204.5, 115.4, 31.2, 68.9, 179.5, and 211.1 mm, respectively, following the order C6 > C1 > C5 > C2 > C4 > C3. The sidewall displacements in working conditions C1–C6 are 195.3, 182.6, 59.6, 22.7, 63.8, and 171.5 mm, respectively, following the order C1 > C2 > C6 > C5 > C3 > C4.

(2) When the different parts of the roadway are in the limestone strata, the deformation of the surrounding rock is small, generally within 50 mm; when the different parts of the roadway are in the mudstone strata, the deformation of the surrounding rock is relatively large, generally greater than 150 mm. The average deformation of different parts of the roadway is used as the evaluation standard. The average deformations of different parts in working conditions C1–C6 are 210.6, 155.9, 105.0, 74.9, 125.9, and 166.0 mm, respectively. In working conditions C1, C2, and C6, the average deformations all exceed 150 mm, and the roadway is mainly affected by soft rocks. In working conditions C3, C4, and C5, the average deformations are in the range of 100–150 mm, and the roadway is affected by both soft and hard rocks.

(3) The larger the proportion of the roadway in the hard-rock strata is, the smaller the deformation of the surrounding rock. For example, the roof displacements in working conditions C4–C6 are 9.0, 9.4, and 10.9 mm, respectively, and the roof displacement in working condition C3 and the sidewall displacement in working condition C4 are 33.8 and 22.7 mm, respectively. The larger the proportion of the roadway in the soft rock is, the larger the deformation of the surrounding rock. For example, the roof displacements in working conditions C5 and C6 reach 250.7 and 270.5 mm, respectively, and the floor displacements in working conditions C2 and C3 reach 278.5 and 295.2 mm, respectively.

3.2.2. Comparative of Plastic Zones of the Surrounding Rock under Different Working Conditions. Figure 7 shows the calculation ranges of the plastic zones of the surrounding rock under different working conditions. Figure 8 shows the distribution of the plastic zones of the surrounding rock under different working conditions.

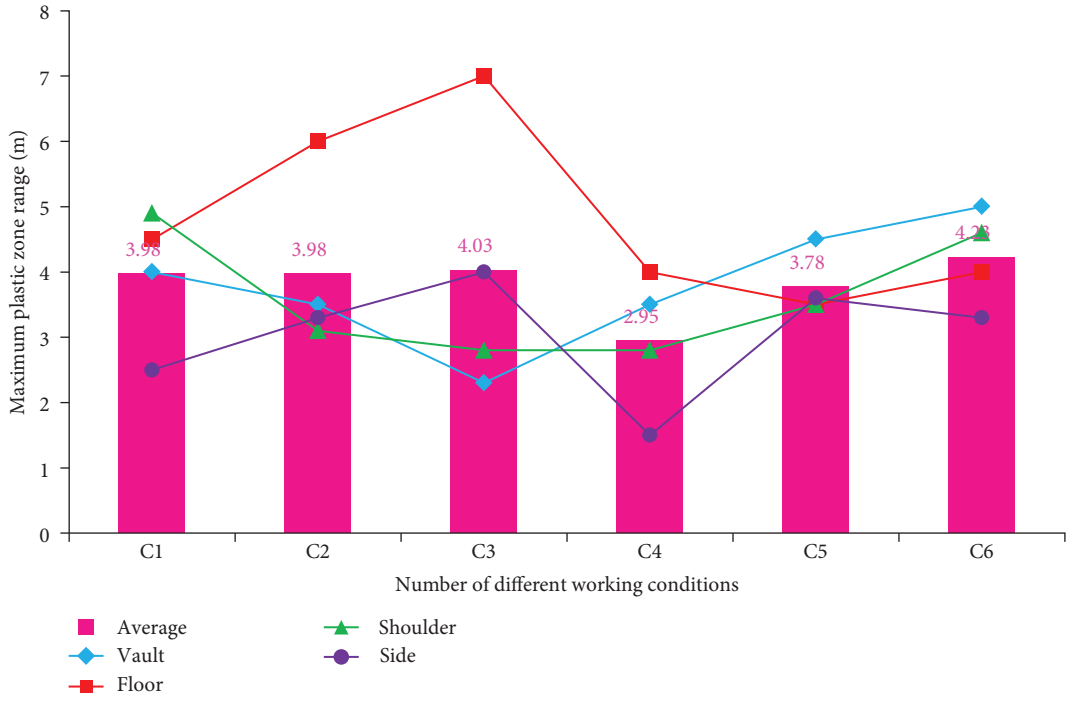

Figure 7: Maximum plastic range of different working conditions.

The comparative analysis shows that:

(1) The plastic zone variation patterns of the surrounding rock of the roadway under different working conditions are different. The plastic zone ranges of the roof in the working conditions C1–C6 are 4.0, 3.5, 2.3, 3.5, 4.5, and 5.0 m, respectively, following the order C6 > C5 > C1 > C4 = C2 > C3. The plastic zone ranges of the floor in the working conditions C1–C6 are 4.5, 6.0, 7.0, 4.0, 3.5, and 4.0 m, respectively, following the order C3 > C2 > C1 > C4 = C6 > C5. The plastic zone ranges of the shoulder are 4.9, 3.1, 2.8, 2.8, 3.5, and 4.6 m, respectively, following the order C1 > C6 > C5 > C2 > C3 = C4. The plastic zone ranges of the sidewalls are 2.5, 3.3, 4.0, 1.5, 3.6, and 3.3 m, respectively, following the order C3 > C5 > C2 = C6 > C1 > C4.

(2) The plastic zone of the rock surrounding the roadway is dominated by tensile–shear failure mainly because the shallow rock surrounding the roadway is in a state of approximately unidirectional stress to bidirectional stress, but the surrounding rock is overall dominated by compression–shear failure. Under high stress, the plastic zone range of the surrounding rock is relatively large. The average plastic zone range of the different parts of the roadway is used as the evaluation standard. The average plastic zone ranges of the different parts of the roadway in working conditions C1–C6 are 3.98, 3.98, 4.03, 2.95, 3.78, and 4.23 m, respectively, all exceeding the bolt length. The plastic zone ranges of some parts approach or exceed the cable length. For example, the plastic zone ranges of the floor in working conditions C2 and C3 are 6 and 7 m, respectively.

(3) During roadway excavation, the roadway in soft- and hard-interbedded rock strata has an asymmetrical plastic zone, and the morphology of the plastic zone of the surrounding rock at the interface between soft and hard rocks undergoes abrupt changes. For example, in working condition C1, when the plastic zone enters the hard rock from the soft rock, the plastic zone becomes narrower and smaller; in working condition C4, when the plastic zone enters the soft rock from the hard rock, the plastic zone has a relatively uniform morphological distribution and a relatively large range. In general, the plastic zone has a larger range in the soft rock than in the hard rock.

3.3. Analysis on Deformation and Failure Mechanisms of the Surrounding Rock of Deep Cross-Measure Roadway. Based on the numerical analysis results of different working conditions, the on-site geological conditions of the roadway, and the monitoring and analysis of the original support scheme, the deformation and failure mechanisms of the surrounding rock of the deep cross-measure roadway are summarized as follows:

(1) The roadway has a large burial depth, high ground stress, and a large angle between the maximum principal stress and the roadway. This region is dominated by horizontal stress, with a maximum horizontal stress of 37.1 MPa, and the lateral pressure coefficient is 1.58. This roadway is a typical high-stress roadway

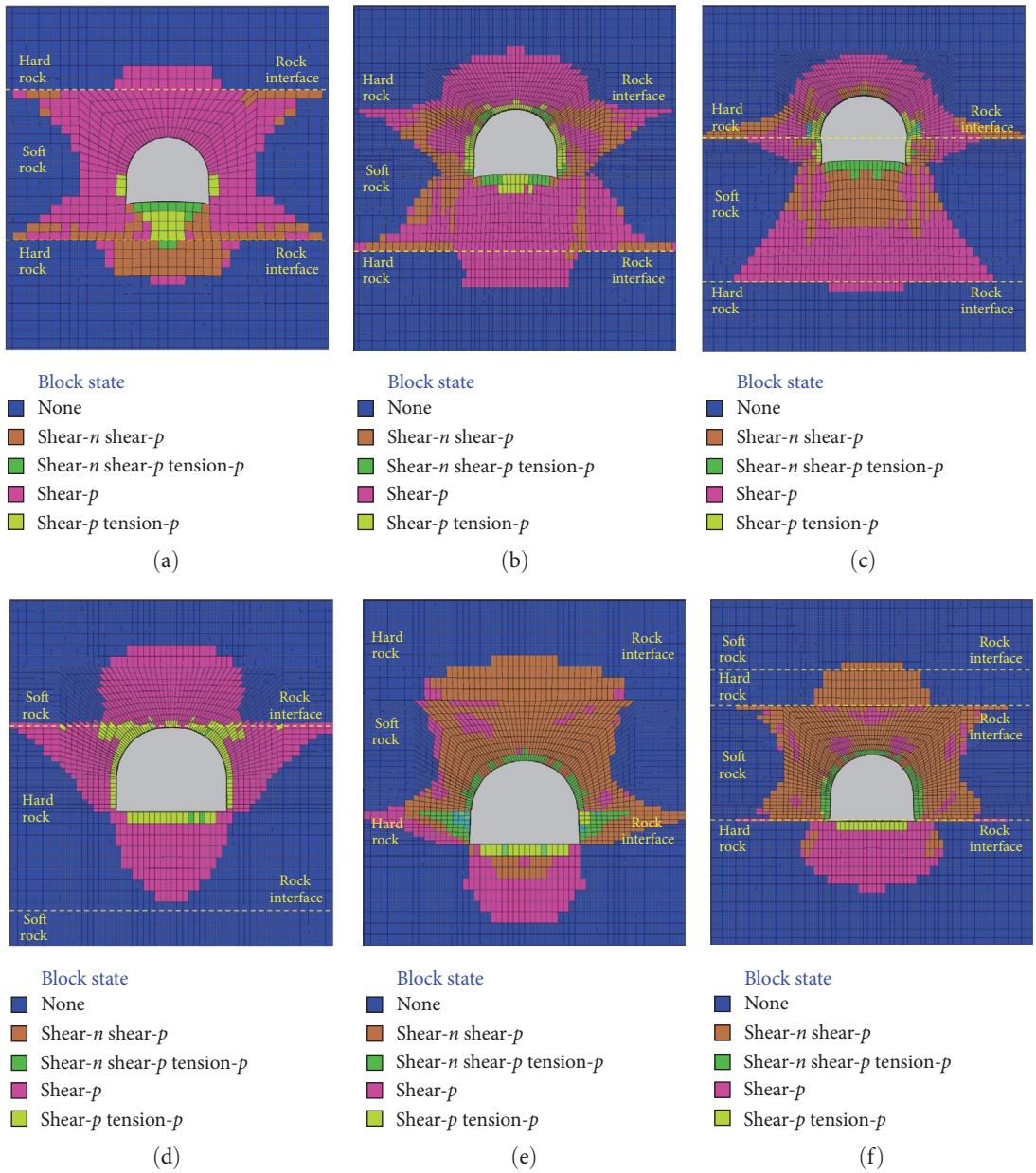

Figure 8: Distribution of plastic zone of different working conditions. (a) C1, (b) C2, (c) C3, (d) C4, (e) C5, and (f) C6.

dominated by tectonic stress, which results in a large overall failure range of the roadway. In addition, the angle between the maximum horizontal principal stress and the axial direction of the roadway is ~60°, which is not conducive to the stability control of the surrounding rock. This angle is one of the main controlling factors that directly cause the large deformation of the roadway surrounding rock and the failure of the surrounding rock support system.

(2) During roadway excavation, different parts of the roadway in soft- and hard-interbedded rock strata show greatly different lithological properties. During roadway excavation, the number 1 track main roadway passed through the number 5 limestone, mudstone, and number 3 limestone strata in turn. Therefore, the roof, sidewalls, and floor are in different rock strata, which results in significant differences in deformation and failure characteristics between different parts of the roadway. First, the difference in soft- and hard-rock properties between different strata results in a large difference in the bearing capacities of the corresponding surrounding rock, which is also the main reason for the significant difference in morphology between the plastic zones of the roadway under different working conditions. Second, the soft- and hard-rock interfaces are prone to shear failure and abrupt changes in the plastic zone range due to the low bond strength between soft and hard rocks. This phenomenon is especially

Table 3: Data of evaluation indices and quantitative scores.

Scoring indicators	Evaluation score				
	2	4	6	8	10
Surrounding rock deformation (mm)	<50	50–100	100–150	150–200	≥200
Plastic range (m)	<2	2–3	3–4	4–5	≥5

prominent in the mudstone strata, manifesting as large roof or floor deformations in these strata.

(3) The original support scheme of the roadway does not work well for the surrounding rock, and its support bearing capacity is therefore low. The original support scheme adopts a symmetrical arrangement of bolt–mesh–cable–shotcrete support, which cannot achieve a structural coupling effect with the soft- and hard-interbedded rock strata. As a result, the stress distribution in the surrounding rock cannot be homogenized, causing local stress concentration and resulting in support failures (such as spray layer cracking and bolt breakage). In addition, the lack of floor reinforcement measures causes the floor to become the main area of stress release, and large deformations (such as severe floor heave) occur in the mudstone strata. Furthermore, the mudstone has a high clay mineral content, and the numbers 3 and 5 limestone strata are aquifers. The mudstone expands after absorbing water, which further intensifies roadway deformation and failure.

4. Stability Evaluation and Control Countermeasures of a Deep Cross-Measure Roadway

4.1. Classification of Roadway Stability and Control Countermeasures. Under cross-measure conditions, the deformation and failure of each part of the roadway are affected by the lithological properties and ranges of the strata. The use of a single indicator to evaluate the stability of the surrounding rock has limitations and is not comprehensive, while the use of too many indicators to evaluate the stability of the surrounding rock is overly complex. Based on the numerical analysis in Section 3, two types of evaluation indicators (i.e., the surrounding rock deformations and plastic ranges in the roof, shoulder, floor, and sidewalls of the roadway) are selected in this section, quantitatively assessed based on a ten-point system, and then classified into five levels. Based on our practice of controlling the surrounding rock stability of a large number of roadways in the Juye coalfield [20–23], the classification scheme is determined, as shown in Table 3.

The analytic hierarchy process (AHP) is used to evaluate and analyze the surrounding rock stability under different working conditions, and the basic AHP model is established:

$$g_j = \sum_{i=1}^{n} \omega_{ij} c_{ij} \tag{1}$$

Table 4: Grading standards.

g_j	0–2.5	2.5–5	5–7.5	7.5–10
Stability grade	Stable	Basically stable	Instable	Extremely unstable

Table 5: Judgment matrix for A–B.

A	B_1	B_2	W	Indicators
B_1	1	1.73	0.63	$\lambda_{max} = 2$; CI = 0
B_2	0.58	1	0.37	RI = 0; CR = 0 < 0.1

Table 6: Judgment matrix for B_1–b.

B_1	b_{11}	b_{12}	b_{13}	b_{14}	W	Indicators
b_{11}	1	1.73	2.28	3	0.42	$\lambda_{max} = 4.02$
b_{12}	0.58	1	1.73	2.28	0.28	CI = 0.067
b_{13}	0.44	0.58	1	1.73	0.18	RI = 0.89
b_{14}	0.33	0.44	0.58	1	0.12	CR = 0.0075 < 0.1

Table 7: Judgment matrix for B_2–b.

B_2	b_{21}	b_{22}	b_{23}	b_{24}	W	Indicators
b_{21}	1	1.32	3	3.95	0.43	$\lambda_{max} = 4.02$
b_{22}	0.76	1	1.73	2.28	0.29	CI = 0.0067
b_{23}	0.33	0.58	1	1.73	0.17	RI = 0.89
b_{24}	0.25	0.44	0.58	1	0.11	CR = 0.0075 < 0.1

where c_{ij} is the score of the ith factor of the jth cross-measure roadway; and ω_{ij} is the weight of the ith factor of the jth cross-measure roadway. Based on the on-site roadway support control in the Juye coalfield, the weighted average g_j, that is, the stability of the surrounding rock of the corresponding cross-measure roadway, is divided into four levels, as shown in Table 4.

Tables 5–8 show the judgment matrices for the stability of the surrounding rock of the cross-measure roadway. When the CR is less than 0.1, the matrices have satisfactory consistency.

$$\mathrm{CI} = \sum_{i=1}^{n} B_i \mathrm{CI}_i = 0.63 \times 0.067 + 0.37 \times 0.0067 = 0.0067 \tag{2}$$

Table 8: The weight of each element for target stratum.

b	B_1 0.63	B_2 0.37	Weight
b_{11}	0.42		0.2646
b_{12}	0.28		0.1764
b_{13}	0.18		0.1134
b_{14}	0.12		0.0756
b_{21}		0.43	0.1591
b_{22}		0.29	0.1073
b_{23}		0.17	0.0629
b_{24}		0.11	0.0407

Table 9: Stable classification and proposed supporting program.

Working condition	Comprehensive evaluation value	Stability grade	Control countermeasures	Grouting position
C1	8.946	Extremely unstable	Full section anchor bolt + roof anchor cable + full section grouting	Full section
C2	5.798	Instable	Full section anchor bolt + roof anchor cable + half section grouting	Side + floor
C3	4.3386	Basically stable	Full section anchor bolt + roof anchor cable + key position grouting	Floor
C4	5.1688	Instable	Full section anchor bolt + roof anchor cable + half section grouting	Roof + shoulder
C5	7.1246	Instable	Full section anchor bolt + roof anchor cable + half section grouting	Roof + shoulder
C6	8.4384	Extremely unstable	Full section anchor bolt + roof anchor cable + full section grouting	Full section

$$\mathrm{RI} = \sum_{i=1}^{n} B_i \mathrm{RI}_i = 0.63 \times 0.89 + 0.37 \times 0.89 = 0.89 \quad (3)$$

$$\mathrm{CR} = \frac{\mathrm{CI}}{\mathrm{RI}} = \frac{0.0067}{0.89} = 0.0075 < 0.1. \quad (4)$$

Equation (1) is used to calculate the comprehensive evaluation value and level of the cross-measure roadway stability under different working conditions. Based on the deformation and failure patterns of each part of the roadway in Section 3, grouting reinforcement-based targeted control countermeasures are designed, as shown in Table 9.

Specificly, as shown in Figure 9, the bolt model of roadway roof and sidewalls is $\Phi 22 \times 2{,}400$ mm with interrow spacing of 800×800 mm, and the bolt model of floor $\Phi 22 \times 2{,}000$ mm with interrow spacing of $1{,}600 \times 1{,}600$ mm. The cable model is $\Phi 18 \times 6{,}200$ mm with interrow spacing of $1{,}600 \times 1{,}600$ mm with 5 in each row. Grouting bolt model of roadway roof and sidewalls is $\Phi 32 \times 2{,}500$ mm with interrow spacing of $1{,}200 \times 1{,}600$ mm, and grouting bolt model of floor $\Phi 32 \times 2{,}000$ mm with interrow spacing of $1{,}600 \times 1{,}600$ mm.

4.2. Analysis on the Effect of Surrounding Rock Control Countermeasures of Deep Cross-Measure Roadway. Figures 10–12 show the calculated control effects of the roadway surrounding rock stability under different working conditions after the control countermeasures in Section 4.1 are adopted.

The comparative analysis shows that:

(1) After the proposed control countermeasures are adopted, the average deformations of different parts in working conditions C1–C6 are 72.7, 64.6, 44.6, 24.2, 60.9, and 65.2 mm, respectively (all values are essentially between 20 and 70 mm), which are lower than those of the original regime by 65.5%, 58.6%, 57.5%, 67.7%, 51.6%, and 60.7% (all higher than 50%), respectively. The overall roadway deformation is effectively controlled.

(2) After adopting the proposed control countermeasures, the average plastic zone ranges of different parts of the roadway in working conditions C1–C6 are 1.98, 2.6, 1.98, 1.6, 1.28, and 1.63 m, respectively, which are less than those of the original regime by 50.3%, 34.6%, 50.9%, 45.8%, 66.2%, and 61.5%, respectively. Therefore, the proposed control countermeasures can provide a stable anchorage foundation for bolt and cable support. Under working conditions C1–C6, the morphological distributions of the plastic zones in different parts of the roadway are relatively uniform, the expansion of the plastic zone is suppressed, and the abrupt changes in the

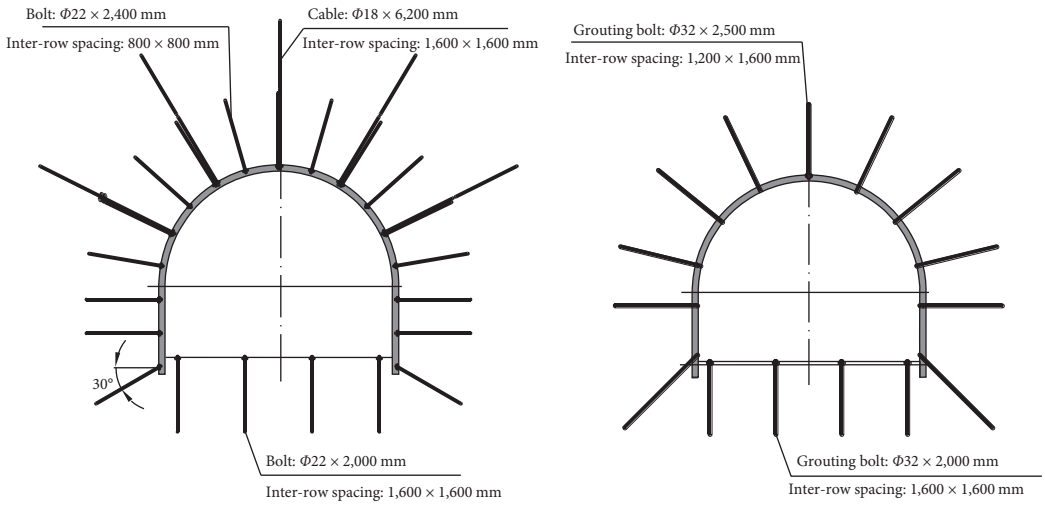

Figure 9: Proposed support schemes. (a) Bolt and cable support scheme and (b) grouting scheme.

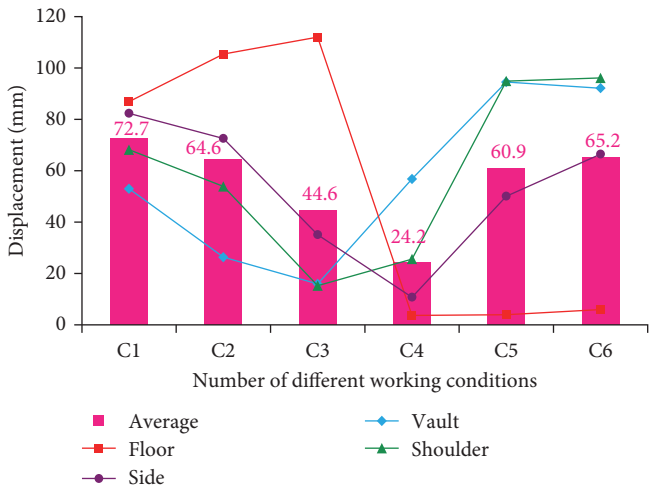

Figure 10: Maximum displacement of different working conditions under proposed control countermeasures.

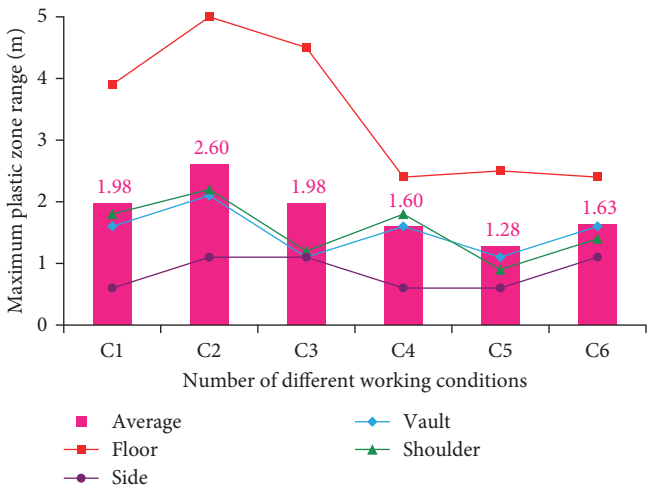

Figure 11: Maximum plastic range of different working conditions under proposed control countermeasures.

plastic zone at the soft- and hard-rock interfaces are significantly reduced.

4.3. Field Application of Surrounding Rock Control in Deep Cross-Measure Roadway. The number 1 track main roadway in Section 2.1 was selected as the field test roadway, and the control countermeasures proposed in Section 4.1 were used for different working conditions. The convergence of the roadway section was monitored, and the control effect of the surrounding rock stability was analyzed. Figure 13 shows a sketch of roadway deformations after 90 days of monitoring for working conditions C1 and C6 with the proposed control countermeasures implemented.

Under working condition C1, the obvious deformations (maximum deformation of 71 mm) in the test section occurred at the floor of the roadway, and the roof subsidence was not obvious. On the 90th day of monitoring, the average deformation of the measurement sites was 57.8 mm, which was 75.1% less than the original deformation, compared with Figure 2(b). The obvious deformations (maximum deformation of 73 mm) of the test section under working condition C6 occurred at the roof of the roadway. The deformations at the left and right sides of the floor were significantly reduced. On the 90th day of monitoring, the average deformation of the measurement sites was 47.4 mm, which was 77.2% less than the original deformation, compared with Figure 2(c). These results indicate that the stability of the surrounding rock of the cross-measure roadway was effectively controlled by the scheme proposed in this paper.

5. Conclusions

(1) Under the original support scheme of deep cross-measure roadway of the Wanfu coal mine, the degree

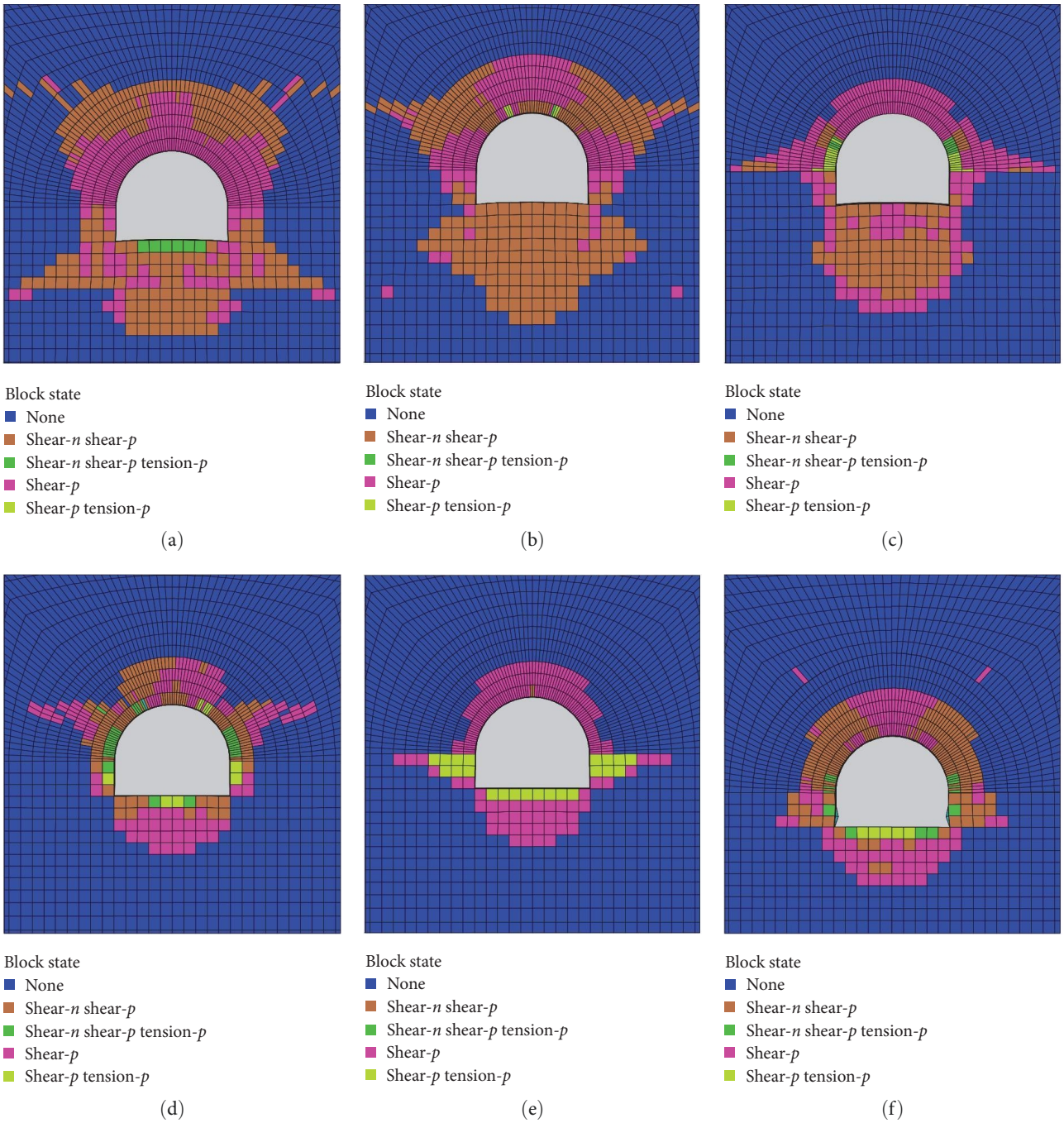

Figure 12: Distribution of plastic zone of different working conditions under proposed control countermeasures. (a) C1, (b) C2, (c) C3, (d) C4, (e) C5, and (f) C6.

of deformation and failure of the surrounding rock varies under different working conditions, the roadway in the limestone interval had an average surrounding rock deformation of 16 mm, and 232.8 mm in the mudstone interval; the damage range of the roadway in the mudstone interval exceeded the length of the bolt, and the damage range in some locations even exceeded the length of the cable; failures of support components occurred frequently, the stability control requirements of surrounding rock could not be meet.

(2) The numerical comparative tests under different working conditions are carried out, The roof, floor, shoulder, and sidewalls of the roadway are located in different rock strata under different working conditions, which results in inconsistent surrounding rock deformation patterns at different parts of the roadway. The plastic zone of the rock surrounding the roadway is dominated by tensile–shear failure, during roadway excavation, the roadway in soft- and hard-interbedded rock strata has an asymmetrical plastic zone, and the morphology of the plastic

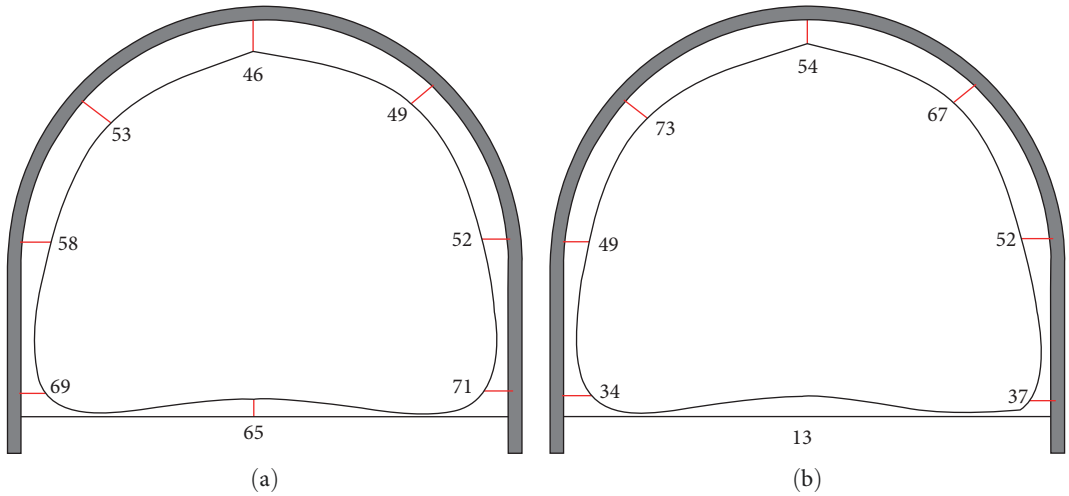

Figure 13: Roadway final shape of working conditions (a) C1 and (b) C6.

zone of the surrounding rock at the interface between soft and hard rocks undergoes abrupt changes. The deformation and failure mechanisms of the surrounding rock of the deep cross-measure roadway are summarized: the roadway has a large burial depth, high ground stress, and a large angle between the maximum principal stress and the roadway; during roadway excavation, different parts of the roadway in soft- and hard-interbedded rock strata show greatly different lithological properties; the original support scheme of the roadway does not work well for the surrounding rock, and its support bearing capacity is therefore low.

(3) The surrounding rock stability evaluation model of cross-measure roadway is established, two types of evaluation indicators, that is, the deformations of the surrounding rock and the plastic ranges in the four typical parts (roof, shoulder, floor, and sidewalls) of the roadway were selected to rate the stability of the roadway, grouting reinforcement-based targeted control countermeasures are designed, numerical analysis and field application of these control countermeasures were carried out to solve the problem of controlling the surrounding rock stability of deep cross-measure roadways.

Data Availability

The data used to support the findings of this study are included within the article.

Conflicts of Interest

The authors declare that they have no conflicts of interest.

Acknowledgments

This work was supported by the National Natural Science Foundation of China (grant numbers 51904006, 51874188, and 51704125) and Anhui Provincial Key Research and Development Program (grant number 202104a07020019).

References

[1] Q. Wang, M. He, J. Yang, H. Gao, B. Jiang, and H. Yu, "Study of a no-pillar mining technique with automatically formed gob-side entry retaining for longwall mining in coal mines," *International Journal of Rock Mechanics and Mining Sciences*, vol. 110, pp. 1–8, 2018.

[2] Q. Wang, H. Gao, H. Yu, B. Jiang, and B. Liu, "Method for measuring rock mass characteristics and evaluating the grouting-reinforced effect based on digital drilling," *Rock Mechanics and Rock Engineering*, vol. 52, no. 3, pp. 841–851, 2019.

[3] Q. Wang, Z. Jiang, B. Jiang, H. Gao, Y. Huang, and P. Zhang, "Research on an automatic roadway formation method in deep mining areas by roof cutting with high-strength bolt-grouting," *International Journal of Rock Mechanics and Mining Sciences*, vol. 128, p. 104264, 2020.

[4] F. Huang, Y. Zhou, T. Li, and X. Hu, "Laboratory experimental study on mechanical properties and failure modes of soft and hard interbedded rock mass," *Journal of China Coal Society*, vol. 45, no. S1, pp. 230–238, 2020.

[5] X. Liu, B. Xu, X. Zhou, L. Yi, X. Zeng, and J. Wang, "Investigation on the macro-meso shear mechanical properties of soft-hard interbedded rock discontinuity," *Journal of China Coal Society*, vol. 46, no. 9, pp. 2895–2909, 2021.

[6] A. Li, G. J. Shao, H. L. Fan, P. R. Du, and Y. H. Zhu, "Investigation of mechanical properties of soft and hard interbedded composite rock mass based on meso-level heterogeneity," *Chinese Journal of Rock Mechanics and Engineering*, vol. 33, no. S1, pp. 3042–3049, 2014.

[7] C. Yao, Y. Li, Q. Jiang, and C. Zhou, "Mesoscopic model of failure process of interlayered rock under compression," *Chinese Journal of Rock Mechanics and Engineering*, vol. 34, no. 8, pp. 1542–1551, 2015.

[8] Q.-s. Huang and J.-l. Cheng, "Research on stress distribution and failure characteristics of coal mining floor in soft-hard alternant strata," *Rock and Soil Mechanics*, vol. 38, no. S1, pp. 36–42, 2017.

[9] N. Barton and E. Grimstad, "Rock mass conditions dictate choice between NMT and NATM," *Tunnels and Tunneling*, vol. 13, no. 1, pp. 14–18, 1994.

[10] Z. T. Bieniawski, *Engineering Rock Mass Classification—A Complete Manual for Engineers and Geologists in Mining, Civil and Petroleum engineering*, p. 56, Wiley and Sons, New York, 1989.

[11] M. Wang, Y. Zhu, Y. Li, D. Guo, W. Li, and M. Wang, "Study on stability classification of surrounding rock of coal gateway based on fuzzy clustering method," *Journal of Mining Science and Technology*, vol. 3, no. 3, pp. 238–245, 2018.

[12] Y. D. Zhu and W. T. Ma, "Method of support vector machines for classifying surrounding rocks of gateways," *Journal of Mining and Safety Engineering*, vol. 23, no. 3, pp. 362–365, 2006.

[13] J. K. Jiao, Z. Zhang, L. X. Yan, Y. Q. Zhou, J. B. Li, and Q. L. Cui, "Stability quantitative evaluation and grading support technology of roadway surrounding rock in small and medium coal mine," *Journal of Mining and Safety Engineering*, vol. 39, no. 3, pp. 598–606, 2022.

[14] X. Y. Liu, Y. C. Ye, Y. Liu, Q. H. Wang, N. Yao, and Y. B. Shi, "On the roadway stability and reliability evaluation based on the uncertainty measuring theory," *Journal of Mining and Safety Engineering*, vol. 17, no. 1, pp. 26–31, 2017.

[15] S. Yu and X. Peng, "New method for evaluation of surrounding rock stability in galleries of coal mine," *Journal of China Coal Society*, vol. 18, no. 5, pp. 5–11, 1993.

[16] S. Y. Sun, C. Z. Zhao, Y. Zhang et al., "The deformation characteristics of surrounding rock of crossing roadway in multiple seams under repeated mining and its repair and reinforcement technology," *Journal of Mining and Safety Engineering*, vol. 37, no. 4, pp. 681–688, 2020.

[17] F. Yang, W. Chen, P.-Q. Zheng, G.-J. Wu, J. Yuan, and J. Yu, "Research on mechanism of deformation and failure for steeply inclined roadways in soft–hard alternant strata and its support technology," *Rock and Soil Mechanics*, vol. 35, no. 8, pp. 2367–2425, 2014.

[18] J. Wang, Z. B. Guo, F. Cai, Y. Hao, and X. Liu, "Study on the asymmetric deformation mechanism and control counter-measures of deep layers roadway," *Journal of Mining and Safety Engineering*, vol. 31, no. 1, pp. 28–33, 2014.

[19] H.-s. Jia, N.-j. Ma, and Q.-k. Zhu, "Mechanism and control method of roof fall resulted from butterfly plastic zone penetration," *Journal of China Coal Society*, vol. 41, no. 6, pp. 1384–1392, 2016.

[20] R. Pan, L. Wang, Y. Cai et al., "Analysis of flat roof stability in deep roadway and its repair control," *Journal of Mining and Safety Engineering*, vol. 38, no. 4, pp. 756–765, 2021.

[21] R. Pan, Q. Wang, B. Jiang et al., "Failure of bolt support and experimental study on the parameters of bolt-grouting for supporting the roadways in deep coal seam," *Engineering Failure Analysis*, vol. 80, pp. 218–233, 2017.

[22] Q. Wang, R. Pan, S. C. Li, H. T. Wang, and B. Jiang, "The control effect of surrounding rock with different combinations of the bolt anchoring lengths and pre-tightening forces in underground engineering," *Environmental Earth Sciences*, vol. 77, no. 13, pp. 1–14, 2018.

[23] Q. Wang, B. Jiang, R. Pan et al., "Failure mechanism of surrounding rock with high stress and confined concrete support system," *International Journal of Rock Mechanics and Mining Sciences*, vol. 102, pp. 89–100, 2018.

[24] Z.-q. Zhang, M.-d. Xu, and Q.-s. Liu, "The research on the methodology of weighted average evaluation for surrounding rock stability of tunnel," *Rock and Soil Mechanics*, vol. 30, no. 11, pp. 3464–3468, 2009.